Version 04 as of April 15, 2020
Primary authors: Carlos Yero, Werner Boeglin, Mark Jones
To be submitted to PRL
Comment to cyero002@fiu.edu, boeglinw@fiu.edu, jones@jlab.org by May 01, 2020
INTERNAL DOCUMENT – NOT FOR PUBLIC DISTRIBUTION

Deuteron Electro-Disintegration at Very High Missing Momenta

C. Yero[1], D. Abrams[2], Z. Ahmed[3], A. Ahmidouch[4], B. Aljawrneh[4], S. Alsalmi[5], R. Ambrose[3], W. Armstrong[6], A. Asaturyan[7], K. Assumin-Gyimah[8], C. Ayerbe Gayoso[9], A. Bandari[9], J. Bane[10], S. Basnet[3], V.V. Berdnikov[11], J. Bericic[15], H. Bhatt[8], D. Bhetuwal[8], D. Biswas[12], W. Boeglin[1], P. Bosted[9], E. Brash[13], M. Bukhari[14], H. Chen[2], J.P. Chen[15], M. Chen[2], M.E. Christy[12], S. Covrig[15], K. Craycraft[10], S. Danagoulian[4], D. Day[2], M. Diefenthaler[15], M. Dlamini[16], J. Dunne[8], B. Duran[6], D. Dutta[8], R. Ent[15], R. Evans[3], H. Fenker[15], N. Fomin[10], E. Fuchey[17], D. Gaskell[15], T.N. Gautam[12], F.A. Gonzalez[18], O. Hansen[15], F. Hauenstein[19], A.V. Hernandez[11], T. Horn[11], G. Huber[3], M.K. Jones[15], S. Joosten[6], M.L. Kabir[8], A. Karki[8], C.E. Keppel[15], A. Khanal[1], P. King[16], E. Kinney[20], N. Lashley-Colthirst[12], S. Li[21], W.B. Li[9], A.H. Liyanage[12], D. Mack[15], S. Malace[15], J. Matter[2], D. Meekins[15], R. Michaels[15], A. Mkrtchyan[7], H. Mkrtchyan[7], S.J. Nazeer[12], G. Niculescu[22], M. Niculescu[22], D. Nguyen[2], N. Nuruzzaman[23], B. Pandey[12], S. Park[18], C.F. Perdrisat[9], E. Pooser[15], M. Rehfuss[6], J. Reinhold[1], B. Sawatzky[15], G. Smith[15], A. Sun[24], H. Szumila-Vance[15], V. Tadevosyan[7], S.A. Wood[15], and J. Zhang[18]

[1] *Florida International University, University Park, Florida 33199, USA*
[2] *University of Virginia, Charlottesville, Virginia 22903, USA*
[3] *University of Regina, Regina, Saskatchewan S4S 0A2, Canada*
[4] *North Carolina Agricultural and Technical State University, Greensboro, North Carolina 27411, USA*
[5] *Kent State University, Kent, Ohio 44240, USA*
[6] *Temple University, Philadelphia, Pennsylvania 19122, USA*
[7] *A.I. Alikhanyan National Science Laboratory (Yerevan Physics Institute), 2 Alikhanian Brothers Street, 0036, Yerevan, Armenia*
[8] *Mississippi State University, Mississippi State, Mississippi 39762, USA*
[9] *The College of William & Mary, Williamsburg, Virginia 23185, USA*
[10] *University of Tennessee, Knoxville, Tennessee 37996, USA*
[11] *Catholic University of America, Washington, DC 20064, USA*
[12] *Hampton University, Hampton, Virginia 23669, USA*
[13] *Christopher Newport University, Newport News, Virginia 23606, USA*
[14] *Jazan University, Jazan 45142, Saudi Arabia*
[15] *Thomas Jefferson National Accelerator Facility, Newport News, Virginia 23606, USA*
[16] *Ohio University, Athens, Ohio 45701, USA*
[17] *University of Connecticut, Storrs, Connecticut 06269, USA*
[18] *Stony Brook University, Stony Brook, New York 11794, USA*
[19] *Old Dominion University, Norfolk, Virginia 23529, USA*
[20] *University of Colorado Boulder, Boulder, Colorado 80309, USA*
[21] *University of New Hampshire, Durham, New Hampshire 03824, USA*
[22] *James Madison University, Harrisonburg, Virginia 22807, USA*
[23] *Rutgers University, New Brunswick, New Jersey 08854, USA and*
[24] *Carnegie Mellon University, Pittsburgh, Pennsylvania 15213, USA*

(Dated: April 15, 2020)

^{2}H$(e,e'p)n$ cross sections have been measured at 4-momentum transfers of $-Q^2 = 4.5 \pm 0.5$ (GeV/c)^2 reaching neutron recoil (missing) momenta up $p_{\rm r} \sim 1.0$ GeV/c. The data have been obtained at fixed neutron recoil angles $\theta_{nq} = 35^\circ$, 45° and 75° with respect to the 3-momentum transfer $\vec{q}$. The new data agrees well with previous data which reached $p_{\rm r} \sim 500$ MeV/c. At $\theta_{nq} = 35^\circ$ and 45°, final state interactions (FSI), meson exchange currents (MEC) and isobar configurations (IC) are suppressed and the plane wave impulse approximation (PWIA) provides the dominant cross section contribution. The new data are compared to recent theoretical calculations, where a significant disagreement for missing momenta $p_{\rm r} > 700$ MeV/c has been observed.

The deuteron is the only bound two-nucleon system and serves as a starting point to study the strong nuclear force at the sub-Fermi distance scale, a region which is currently not well understood. At such small internucleon distances, the nucleon-nucleon (NN) interaction is expected to become repulsive and the interacting nucleons begin to overlap. This short distance region is directly related to two-nucleon short range correlations

(SRC) observed in $A > 2$ nuclei [1–6]. Short-range studies of the deuteron are also important in determining whether, or to what extent, the description of nuclei in terms of nucleon/meson degrees of freedom is still valid, before having to include explicit quark degree of freedoms, an issue of fundamental importance in nuclear physics [7]. As of the present time, there are only a few nuclear physics experiments for which a transition between nucleonic to quark degrees of freedom has been observed [8–10].

Within the PWIA, the virtual photon couples to the bound proton which is subsequently ejected from the nucleus without further interaction with the recoiling system (neutron). The neutron carries a recoil momentum, $p_{\rm r}$, equal in magnitude but opposite in direction to the initial state proton, $\vec{p}_{\rm r} \sim -\vec{p}_{{\rm i},p}$, thus providing information on the momentum of the bound nucleon and its momentum distribution. The most direct way to study the short range structure of the deuteron wave function (or equivalently, its high momentum components) is via the exclusive deuteron electro-disintegration reaction at $p_{\rm r} > 300$ MeV/c.

In reality, the ejected nucleon undergoes FSI corresponding to subsequent interactions with the recoiling system. Another possibility is that the photon couples to the virtual meson being exchanged between nucleons (MEC), or that the photon excites a bound nucleon into a resonance state (N^*) which subsequently decays ($N^*N \rightarrow NN$) via FSI to the ground state (IC). FSI, MEC and IC can significantly alter the recoiling neutron momentum thereby obscuring the original momentum of the bound nucleon and reducing the possibility of directly probing the deuteron momentum distribution.

Theoretically, MEC and IC are expected to be suppressed at $Q^2 > 1$ (GeV/c)^2) and Bjorken $x_{\rm Bj} \equiv Q^2/2M_p\omega > 1$, where M_p and ω are the proton mass and photon energy transfer, respectively. The suppression of MEC can be understood from the fact that the estimated MEC scattering amplitude is proportional to $(1 + Q^2/m^2_{\rm meson})^{-2}(1 + Q^2/\Lambda^2)^{-2}$, where $m_{\rm meson} \approx 0.71$ GeV/c^2 and $\Lambda^2 \sim 0.8 - 1$ (GeV/c)^2 [11]. IC can be suppressed kinematically by selecting $x_{\rm Bj} > 1$, where one probes the lower energy (ω) part of the deuteron quasi-elastic peak which is maximally far away from the inelastic resonance electro-production threshold. Previous deuteron electro-disintegration experiments performed at lower Q^2 ($Q^2 < 1$ (GeV/c)^2)(See Section 5 of Ref. [7]) have helped quantify the contributions from FSI, MEC and IC on the $^2{\rm H}(e,e'p)n$ cross-section and to determine the kinematics at which they are either suppressed (MEC and IC) or under control (FSI).

At large Q^2, FSI are described by the General Eikonal Approximation (GEA) [7, 11, 12] which predicts a strong dependence of FSI on neutron recoil angles θ_{nq}. GEA predicts FSI to be maximal for $\theta_{nq} \sim 70^\circ$. This strong angular dependence has been found to lead to the cancellation of FSI at neutron recoil angles around $\theta_{nq} \sim 40^\circ$ and $\theta_{nq} \sim 120^\circ$. Since at $\theta_{nq} \sim 120^\circ$ IC are not negligible, $x_{\rm Bj} > 1$ (or equivalently $\theta_{nq} \sim 40^\circ$) is the preferred choice to suppress IC as well as FSI.

The first $^2{\rm H}(e,e'p)n$ experiments at high Q^2 (> 1 (GeV/c)^2) were carried out at Jefferson Lab (JLab) in Halls A [13] and B [14]. Both experiments determined that the cross-sections for fixed missing momenta indeed exhibited a strong angular dependence with neutron recoil angles, peaking at $\theta_{nq} \sim 70^\circ$ in agreement with GEA [11, 12] calculations. In Hall B, the CEBAF Large Acceptance Spectrometer (CLAS) measured angular distributions for a range of Q^2 values as well as momentum distributions. However, statistical limitations made it necessary to integrate over a wide angular range to determine momentum distributions which are therefore dominated by FSI, MEC and IC for missing momenta above ~ 300 MeV/c.

In Hall A, the pair of high resolution spectrometers (HRS) made it possible to measure the missing momentum dependence of the cross section for fixed neutron recoil angles (θ_{nq}) reaching missing momenta up to $p_{\rm r} = 550$ MeV/c at $Q^2 = 3.5 \pm 0.25$ (GeV/c)^2. For the first time very different momentum distributions were found for $\theta_{nq} = 35 \pm 5^\circ$ and $45 \pm 5^\circ$ compared to $\theta_{nq} = 75 \pm 5^\circ$. Theoretical models attributed this difference to the suppression of FSI at the smaller angles ($\theta_{nq} = 35, 45^\circ$) compared to FSI dominance at $\theta_{nq} = 75^\circ$ [13].

The experiment presented in this Letter takes advantage of the kinematic window previously found in the Hall A experiment and extends the $^2{\rm H}(e,e'p)n$ cross section measurements to $Q^2 = 4.5 \pm 0.5$ (GeV/c)^2 and neutron recoil momenta up to $p_{\rm r} \sim 1$ GeV/c which is almost double of the maximum recoil momentum measured in Hall A [13]. Measurements at such large Q^2 and high missing momenta required scattered electrons to be detected at about 8.5 GeV/c which was only made possible with the newly commissioned Hall C Super High Momentum Spectrometer (SHMS). At the selected kinematic settings with neutron recoil angles between 35° and 45°, MEC and IC are suppressed and FSI are under control giving access to high momentum components of the deuteron wave function.

A 10.6 GeV electron beam was incident on a 10 cm long liquid deuterium target (LD_2). The scattered electron and knocked-out proton were detected in coincidence by the new SHMS and the existing High Momentum Spectrometer (HMS), respectively. The beam currents delivered by the accelerator ranged between 45-60 μA and the beam was rastered over a 2x2 mm^2 area to reduce the effects of localized boiling on the cryogenic targets (hydrogen and deuterium).

Both Hall C spectrometers have similar standard detector packages, each with four scintillator planes [15] used for triggering, a pair of drift chambers [16] used for

tracking, and a calorimeter [17] and gas Čerenkov [18, 19] used for electron identification. For each spectrometer, a logical hardware signal was created from the coincidence of hits in three of the four scintillator planes. The event trigger was the coincidence of these two signals.

We measured three central missing momentum settings: $p_{\rm r}$ = 80, 580 and 750 MeV/c. At each of these settings, the electron arm (SHMS) was fixed and the proton arm (HMS) was rotated from smaller to larger angles corresponding to the the lower and higher missing momentum settings, respectively. At these kinematic settings, the 3-momentum transfer covered a range of $2.4 \lesssim |\vec{q}| \lesssim 3.2$ GeV/c, which is more than twice the highest neutron recoil momentum measured in this experiment. As a result, most of the virtual photon momentum is transferred to the proton which scatters at angles relative to $\vec{q}$ in the range $0.4^\circ \lesssim \theta_{pq} \lesssim 21.4^\circ$. At these forward angles and large momenta transferred to the proton, the process where the neutron is struck by the virtual photon is suppressed.

Hydrogen elastic ^{1}H$(e,e'p)$ data were also taken at kinematics close to the deuteron $p_{\rm r}$ = 80 MeV/c setting for cross-checks with the spectrometer acceptance model using the Hall C Monte Carlo simulation program, SIMC [20]. Additional ^{1}H$(e,e'p)$ data were also taken at three other kinematic settings that covered the SHMS momentum acceptance range for the deuteron and were used for spectrometer optics optimization, momentum calibration and the determination of the spectrometer offsets and kinematic uncertainties [21].

The kinematics of the recoiling neutron was reconstructed using energy-momentum conservation. The recoil momentum is defined as $\vec{p_{\rm r}} = \vec{q} - \vec{p_{\rm f}}$ and the nuclear binding (or "missing") energy as $E_{\rm m} = \omega - T_p - T_{\rm r}$ where $\vec{p_{\rm f}}$ is the final proton momentum, $\vec{q}$ is the 3-momentum transfer and T_p is the final proton kinetic energy. The recoil particle kinetic energy, $T_{\rm r}$, is calculated from the electron and proton 4-momentum vectors assuming an exclusive three-body final state with a recoiling neutron.

Identical event selection criteria were used for the hydrogen and deuteron data. The criteria were determined by making standard cuts on the spectrometer momentum fraction (δ) to select a region for which the reconstruction optics are well known, a cut to restrict the HMS solid angle acceptance to events that passed directly through the collimator and not by re-scattering from the collimator edges, a "missing" energy cut (peak $\sim$ 2.22 MeV for the deuteron) to select true ^{2}H$(e,e'p)n$ coincidences, a coincidence time cut to select true coincidence events, a PID cut on the SHMS calorimeter normalized total track energy to select electrons and not other sources of background (mostly pions), and a cut on the reconstructed HMS and SHMS reaction vertices to select events that originated from the same reaction vertex at the target.

The experimental data yields for both hydrogen and deuteron data were normalized by the total charge and corrected for various inefficiencies. For ^{2}H$(e,e'p)n$, the corrections were as follows: tracking efficiencies (98.9%-HMS, 96.4%-SHMS), total live time (92.3%), proton loss inefficiency due to nuclear interactions in the HMS (4.7%) [21] and target boiling inefficiency (4.2%) [21]. The values in parentheses were averaged over all momentum settings.

For ^{1}H$(e,e'p)$, the corrected data yield was compared to SIMC calculations using Arrington's proton form factor parametrization [22] to check the spectrometer acceptance model. The ratio of data to simulation yield was determined to be $97.6 \pm 0.3\%$ (statistical uncertainty only).

The systematic uncertainties of the measured cross sections were determined from normalization and kinematic uncertainties in the beam energy and spectrometer angle/momentum settings. The individual contributions from normalization uncertainties for each setting were determined to be (on average): tracking efficiencies (0.40%-HMS, 0.59%-SHMS), and target boiling (0.38%) which were added in quadrature and determined to be about 0.81 % per setting. The systematic uncertainties due to proton loss in HMS (0.49%), total live time (3.0%), and total charge (2.0%) were the same for every setting and thus were added (in quadrature) as an overall normalization constant to the final result.

The systematic uncertainties on the cross section due to systematic error on the absolute beam energy and spectrometer angle/momentum settings were determined point-to-point in (θ_{nq}, $p_{\rm r}$) bins for each missing momentum setting, and added in quadrature for overlapping pr bins. For $\theta_{nq} = 35^\circ, 45^\circ$ and 75° (presented in this Letter) the overall kinematic uncertainty varied up to 6.5%. The overall systematic uncertainty in the cross section was determined by the quadrature sum of the normalization and kinematic uncertainties. This result was then added in quadrature to the statistical uncertainty (25-30% on average) to obtain the final uncertainty in the cross section.

The data were radiatively corrected for each bin in $(\theta_{nq}, p_{\rm r})$ by multiplying the measured cross sections by the ratio of the calculated particle yield excluding and including radiative effects. The SIMC simulation code was used for these calculations with the Deuteron Model by Laget including FSI [23]. For each bin in $(\theta_{nq}, p_{\rm r})$, the averaged ^{2}H$(e,e'p)n$ kinematics was calculated and used in the bin centering correction factor defined as: $f_{\rm bc} \equiv \sigma_{\rm avg.kin}/\bar{\sigma}$, where $\sigma_{\rm avg.kin}$ is the cross section calculated at the averaged kinematics and $\bar{\sigma}$ is the cross section averaged over the kinematic bin. The systematic uncertainty associated with the radiative and bin-centering corrections was investigated using the Laget PWIA and FSI models but negligible effects on the cross sections were found.

The experimental and theoretical reduced cross sections were extracted and are defined as follows:

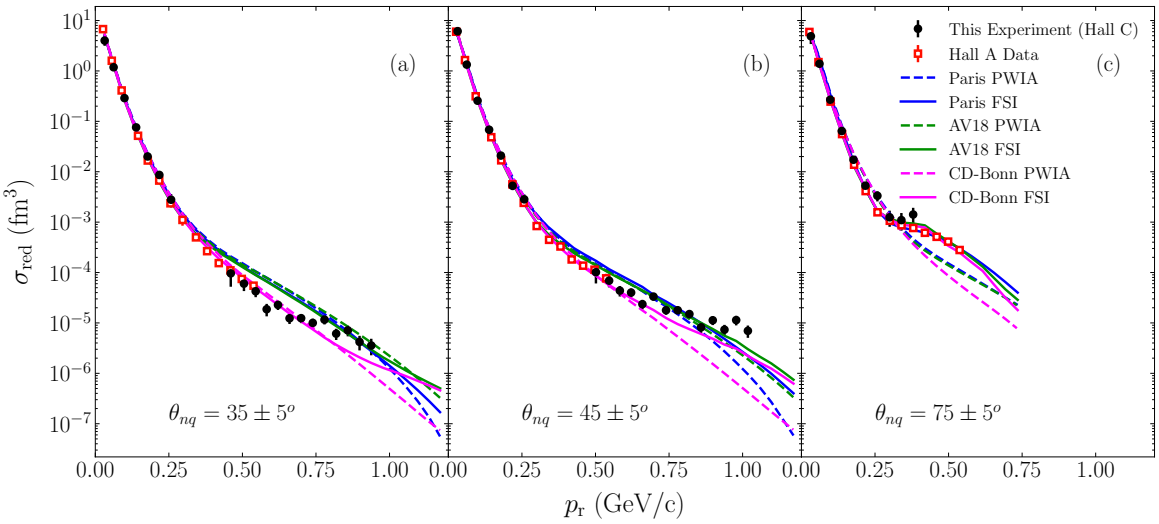

FIG. 1. The reduced cross sections $\sigma_{\rm red}(p_{\rm r})$ as a function of neutron recoil momentum $p_{\rm r}$ are shown in (a)-(c) for recoil angles $\theta_{nq} = 35°, 45°$ and $75°$, respectively, with a bin width of $\pm 5°$. The data is compared to the previous Hall A experiment (red square) results [13] as well as the theoretical reduced cross sections using the Paris(blue), AV18(green) and CD-Bonn(magenta) NN potentials.

$$\sigma_{\rm red} \equiv \frac{\sigma_{\rm exp(th)}}{E_{\rm f} p_{\rm f} f_{\rm rec} \sigma_{\rm cc1}}, \qquad (1)$$

where $\sigma_{\rm exp(th)}$ is the 5-fold experimental (or theoretical) differential cross section, $\frac{d^5\sigma}{d\omega d\Omega_e d\Omega_p}$, $E_{\rm f}$ is the final proton energy, $f_{\rm rec} \equiv \frac{2p_{\rm f}^2 E_{\rm r}}{2p_{\rm f}^2 E_{\rm r} - (q^2 - (p_{\rm f}^2 + p_{\rm r}^2))E_{\rm f}}$ is a recoil factor obtained by integrating over the missing energy of the bound state in the 6-fold differential cross section where $E_{\rm r}$ is the neutron recoil energy, and $\sigma_{\rm cc1}$ is the de Forest [24] electron-proton off-shell cross section calculated using the form factor parametrization of Ref. [22]. Within the PWIA, $\sigma_{\rm red}$ corresponds to the PWIA cross section from the scattering of a proton in the deuteron.

Figure 1 shows the extracted experimental and theoretical reduced cross sections as a function of neutron recoil momentum $p_{\rm r}$ for three recoil angle settings at $Q^2 = 4.5 \pm 0.5$ (GeV/c)^2. For the two highest settings ($p_{\rm r} = 580, 750$ MeV/c), a weighted average of the cross sections were taken in the overlapping regions of $p_{\rm r}$. The results from the previous experiment [13] at a $Q^2 = 3.5 \pm 0.25$ (GeV/c)^2 are plotted as well (red square). The good agreement between the Hall A and C data at lower $p_{\rm r}$ gives us confidence in the measurements made at higher missing momentum settings for which no previous data exist. The data are compared to theoretical reduced cross sections using the charge-dependent Bonn (CD-Bonn) [25], Argonne v_{18} (AV18) [26] and Paris [27] NN-potentials. The theoretical calculations for the CD-Bonn (magenta) and AV18 (green) potentials were performed by Sargsian [28] and those for the Paris potential (blue) were by Laget [23].

For all recoil angles shown in Fig. 1 at recoil momenta $p_{\rm r} \leq 300$ MeV/c, the cross sections are well reproduced by all models when FSI are included. The agreement at $p_{\rm r} \leq 300$ MeV/c can be understood from the fact that this region corresponds to the long-range part of the NN potential where the One Pion Exchange Potential (OPEP) is well known and common to all modern potentials.

Beyond $p_{\rm r} \sim 300$ MeV/c at $\theta_{nq} = 35°$ and $45°$ (Figs. 1(a), 1(b)), the Paris and AV18 models significantly differ from the CD-Bonn. In this region, the Paris/AV18 cross sections are dominated by the PWIA and within good agreement up to $p_{\rm r} \sim 700$ MeV/c. The CD-Bonn cross sections in contrast are generally smaller than the Paris/AV18 in this region. In addition, for $\theta_{nq} = 35°$, they are dominated by the PWIA up to $p_{\rm r} \sim 800$ MeV/c (Fig. 1(a)) while for $\theta_{nq} = 45°$ FSI start to contribute already above 600 MeV/c (Fig. 1(b)). The main difference between the CD-Bonn and Paris/AV18 models is the use of Feynman amplitudes in covariant (original) form by the Bonn group as opposed to local (static) approximations of these amplitudes used by Paris/AV18 groups to describe the NN potential. The effect of these local approximations on the NN potential are shown in Fig. 2 of Ref. [25].

At $\theta_{nq} = 75°$ (Fig. 1(c)) and $p_{\rm r} > 180$ MeV/c, FSI become the dominant contributions to the cross sections for all models which exhibit a similar behaviour (smaller fall-off) that overshadows any possibility of extracting the momentum distributions.

To quantify the discrepancy observed between data

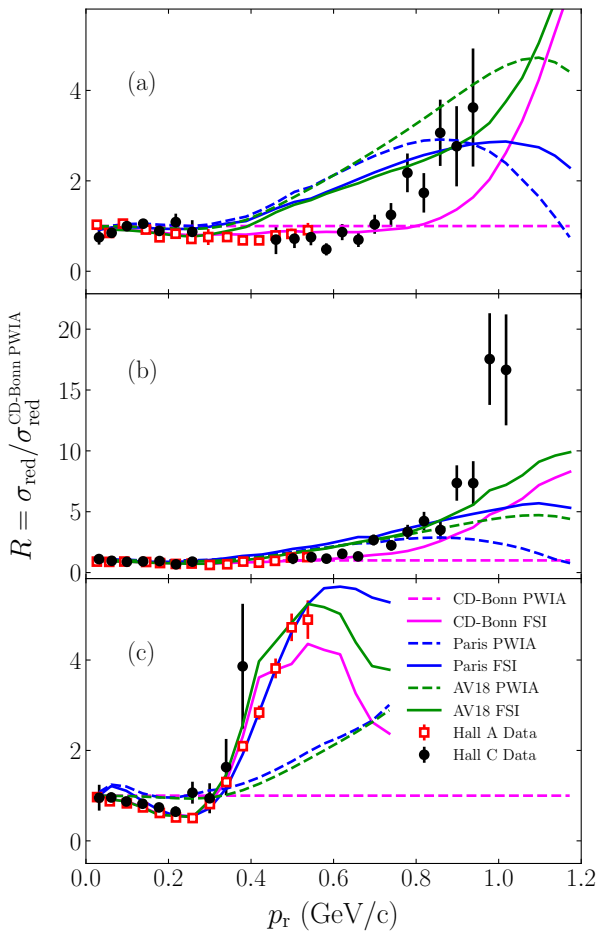

FIG. 2. The ratio $R(p_{\rm r})$ is shown in (a)-(c) for $\theta_{nq} = 35°, 45°$ and $75°$, respectively, each with a bin width of $\pm 5°$. The dashed reference (magenta) line refers to CD-Bonn PWIA calculation (or momentum distribution) by which the data and all models are divided.

and theory in Fig. 1, the ratio of the experimental and theoretical reduced cross sections ($\sigma_{\rm red}$) to the deuteron momentum distribution calculated using the CD-Bonn potential ($\sigma_{\rm red}^{\rm CD\text{-}Bonn\ PWIA}$) [25] is shown in Fig. 2.

For $\theta_{nq} = 35°$ and $45°$ (Figs. 2(a),(b)), the data are best described by the CD-Bonn PWIA calculation for recoil momenta up to $p_{\rm r} \sim 700$ MeV/c and ~ 600 MeV/c, respectively. Furthermore, the agreement between the Halls A and C data solidifies the Hall A approach of selecting a kinematic region where recoil angles are small and FSI are reduced.

At larger recoil momenta, where the ratio is $R > 1$ and increasing, for $\theta_{nq} = 35°$ FSI start to dominate for missing momenta typically above 800 MeV/c for the CD-Bonn calculation while the other models predict still relatively small FSI below 900 MeV/c. At $\theta_{nq} = 45°$ the FSI dominance starts earlier for all models above 800 MeV/c and for the CD-Bonn based calculation above 600 MeV/c.

Overall, it is interesting to note that none of the calculations can reproduce the measured $p_{\rm r}$ dependence above 600 MeV/c in a region where FSI are still relatively small ($< 30\%$). This behavior of the data is new and additional data in this kinematic region are necessary to improve the statistics.

At $\theta_{nq} = 75°$ (Fig. 2(c)), FSI are small below $p_{\rm r} \sim 180$ MeV/c, but do not exactly cancel the PWIA/FSI interference term in the scattering amplitude which results in a small dip in this region in agreement with the data. At $p_{\rm r} > 300$ MeV/c, the data were statistically limited as our focus was on the smaller recoil angles. The Hall A data, however, shows a reasonable agreement with the FSI from all models which gives us confidence in our understanding of FSI at the smaller recoil angles.

This experiment extended the previous Hall A cross section measurements on the ^{2}H$(e,e'p)n$ reaction to very high neutron recoil momenta ($p_{\rm r} > 500$ MeV/c) at kinematics where FSI were expected to be small and the cross section was dominated by PWIA and sensitive to the short range part of the deuteron wavefunction. The experimental reduced cross sections were extracted and found to be in good agreement with the Hall A data. Furthermore, the CD-Bonn model was found to be significantly different than the Paris or AV18 models and was able to partially describe the data over a larger range in $p_{\rm r}$. At higher missing momenta, however, all models were unable to describe the data.

In conclusion, additional measurements of the ^{2}H$(e,e'p)n$ would be required to reduce the statistical uncertainties in this very high missing momentum region ($p_{\rm r} > 500$ MeV/c) to better understand the large deviations observed between the different models and data.

We acknowledge the outstanding support of the staff of the Accelerator and Physics Divisions at Jefferson Lab as well as the entire Hall C staff, technicians, graduate students and users who took shifts or contributed to the equipment for the Hall C upgrade, making all four commissioning experiments possible. This work was supported in part by the U.S. Department of Energy (DOE), Office of Science, Office of Nuclear Physics under grant No. DE-SC0013620 and contract DE-AC05-06OR23177, the Nuclear Regulatory Commission (NRC) Fellowship under grant No. NRC-HQ-84-14-G-0040 and the Doctoral Evidence Acquisition (DEA) Fellowship.

[1] K. S. Egiyan *et al.* (CLAS Collaboration), Observation of nuclear scaling in the $A(e,e')$ reaction at $x_B > 1$, Phys. Rev. C **68**, 014313 (2003).

[2] K. S. Egiyan *et al.* (CLAS Collaboration), Measurement of Two- and Three-Nucleon Short-Range Correlation Probabilities in Nuclei, Phys. Rev. Lett. **96**, 082501 (2006).

[3] R. Shneor *et al.* (Jefferson Lab Hall A Collaboration),

Investigation of Proton-Proton Short-Range Correlations via the ^{12}C$(e, e'pp)$ Reaction, Phys. Rev. Lett. **99**, 072501 (2007).

[4] N. Fomin, D. Higinbotham, M. Sargsian, and P. Solvignon, New Results on Short-Range Correlations in Nuclei, Annual Review of Nuclear and Particle Science **67**, 129159 (2017).

[5] B. Schmookler, M. Duer, A. Schmidt, *et al.*, Modified structure of protons and neutrons in correlated pairs, Nature **566**, 354 (2019), https://doi.org/10.1038/s41586-019-0925-9.

[6] O. Hen, G. A. Miller, E. Piasetzky, and L. B. Weinstein, Nucleon-nucleon correlations, short-lived excitations, and the quarks within, Rev. Mod. Phys. **89**, 045002 (2017), https://link.aps.org/doi/10.1103/RevModPhys.89.045002.

[7] W. Boeglin and M. Sargsian, Modern studies of the Deuteron: From the lab frame to the light front, International Journal of Modern Physics E **24**, 1530003 (2015), https://doi.org/10.1142/S0218301315300039.

[8] C. Bochna *et al.*, Measurements of Deuteron Photodisintegration up to 4.0 GeV, Phys. Rev. Lett. **81**, 4576 (1998).

[9] E. C. Schulte *et al.*, Measurement of the High Energy Two-Body Deuteron Photodisintegration Differential Cross Section, Phys. Rev. Lett. **87**, 102302 (2001).

[10] E. C. Schulte *et al.*, High energy angular distribution measurements of the exclusive deuteron photodisintegration reaction, Phys. Rev. C **66**, 042201 (2002).

[11] M. M. Sargsian, Selected Topics in High Energy Semi-Exclusive Electro-Nuclear Reactions, International Journal of Modern Physics E **10**, 405457 (2001).

[12] L. L. Frankfurt, M. M. Sargsian, and M. I. Strikman, Feynman graphs and generalized eikonal approach to high energy knock-out processes, Phys. Rev. C **56**, 1124 (1997).

[13] W. U. Boeglin *et al.* (For the Hall A Collaboration), Probing the High Momentum Component of the Deuteron at High Q^2, Phys. Rev. Lett. **107**, 262501 (2011).

[14] K. S. Egiyan *et al.* (CLAS Collaboration), Experimental Study of Exclusive ^{2}H$(e, e'p)n$ Reaction Mechanisms at High Q^2, Phys. Rev. Lett. **98**, 262502 (2007).

[15] G. Niculescu, I. Niculescu, M. Burton, D. Coquelin, K. Nisson, and T. Jarell, SHMS Hodoscope Scintillator Detectors, https://hallcweb.jlab.org/document/howtos/shms_scintillator_hodoscope.pdf.

[16] M. Christy, P. Monaghan, N. Kalantarians, D. Biswas, and M. Long, SHMS Drift Chambers, https://hallcweb.jlab.org/document/howtos/shms_drift_chambers.pdf.

[17] H. Mkrtchyan *et al.*, The lead-glass electromagnetic calorimeters for the magnetic spectrometers in Hall C at Jefferson Lab, Nuclear Instruments and Methods in Physics Research Section A: Accelerators, Spectrometers, Detectors and Associated Equipment **719**, 85100 (2013).

[18] W. Li, *Heavy Gas Cherenkov Detector Construction for Hall C at Thomas Jefferson National Accelerator Facility*, Master's thesis, University of Regina (2012).

[19] D. Day, Preliminary Design of the SHMS Noble Cerenkov Detector, https://hallcweb.jlab.org/DocDB/0009/000933/001/shms-cerv6.pdf.

[20] R. Ent, B. W. Filippone, N. C. R. Makins, R. G. Milner, T. G. O'Neill, and D. A. Wasson, Radiative corrections for $(e, e'p)$ reactions at GeV energies, Phys. Rev. C **64**, 054610 (2001), https://link.aps.org/doi/10.1103/PhysRevC.64.054610.

[21] C. Yero, *Cross-Section Measurements of Deuteron Electro-Disintegration at Very High Recoil Momenta and Large* Q^2, Ph.D. thesis, Florida International University, 11200 SW 8th St, Miami, FL 33199 (in progress).

[22] J. Arrington, Implications of the discrepancy between proton form factor measurements, Phys. Rev. C **69**, 022201 (2004).

[23] J. Laget, The electro-disintegration of few body systems revisited, Physics Letters B **609**, 49 (2005).

[24] T. D. Forest, Off-shell electron-nucleon cross sections: The impulse approximation, Nuclear Physics A **392**, 232 (1983).

[25] R. Machleidt, High-precision, charge-dependent Bonn nucleon-nucleon potential, Phys. Rev. C **63**, 024001 (2001).

[26] R. B. Wiringa, V. G. J. Stoks, and R. Schiavilla, Accurate nucleon-nucleon potential with charge-independence breaking, Phys. Rev. C **51**, 38 (1995).

[27] M. Lacombe, B. Loiseau, J. M. Richard, R. V. Mau, J. Côté, P. Pirès, and R. de Tourreil, Parametrization of the Paris $N-N$ potential, Phys. Rev. C **21**, 861 (1980).

[28] M. M. Sargsian, Large Q^2 electrodisintegration of the deuteron in the virtual nucleon approximation, Phys. Rev. C **82**, 014612 (2010).